THE JOURNAL OF BIOLOGICAL CHEMISTRY VOL. 291, NO. 21, pp. 11016–11029, May 20, 2016


# PLEKHA7 Recruits PDZD11 to Adherens Junctions to Stabilize Nectins*

Received for publication, December 27, 2015, and in revised form, April 1, 2016 Published, JBC Papers in Press, April 4, 2016, DOI 10.1074/jbc.M115.712935

**Diego Guerrera[‡§], Jimit Shah[‡§], Ekaterina Vasileva[‡§], Sophie Sluysmans[‡§], Isabelle Méan[‡§], Lionel Jond[‡§], Ina Poser[¶1], Matthias Mann[‖], Anthony A. Hyman[¶1], and Sandra Citi[‡§2]**

*From the [‡]Department of Cell Biology and [§]Institute for Genetics and Genomics in Geneva (iGE3), University of Geneva, 1211-4 Geneva, Switzerland, the [¶]Max Planck Institute for Cell Biology and Genetics, 01307 Dresden, Germany, and the [‖]Max Planck Institute for Biochemistry, 82152 Martinsried, Germany*

**PLEKHA7 is a junctional protein implicated in stabilization of the cadherin protein complex, hypertension, cardiac contractility, glaucoma, microRNA processing, and susceptibility to bacterial toxins. To gain insight into the molecular basis for the functions of PLEKHA7, we looked for new PLEKHA7 interactors. Here, we report the identification of PDZ domain-containing protein 11 (PDZD11) as a new interactor of PLEKHA7 by yeast two-hybrid screening and by mass spectrometry analysis of PLEKHA7 immunoprecipitates. We show that PDZD11 (17 kDa) is expressed in epithelial and endothelial cells, where it forms a complex with PLEKHA7, as determined by co-immunoprecipitation analysis. The N-terminal Trp-Trp (WW) domain of PLEKHA7 interacts directly with the N-terminal 44 amino acids of PDZD11, as shown by GST-pulldown assays. Immunofluorescence analysis shows that PDZD11 is localized at adherens junctions in a PLEKHA7-dependent manner, because its junctional localization is abolished by knock-out of PLEKHA7, and is rescued by re-expression of exogenous PLEKHA7. The junctional recruitment of nectin-1 and nectin-3 and their protein levels are decreased via proteasome-mediated degradation in epithelial cells where either PDZD11 or PLEKHA7 have been knocked-out. PDZD11 forms a complex with nectin-1 and nectin-3, and its PDZ domain interacts directly with the PDZ-binding motif of nectin-1. PDZD11 is required for the efficient assembly of apical junctions of epithelial cells at early time points in the calcium-switch model. These results show that the PLEKHA7-PDZD11 complex stabilizes nectins to promote efficient early junction assembly and uncover a new molecular mechanism through which PLEKHA7 recruits PDZ-binding membrane proteins to epithelial adherens junctions.**

The molecular organization of cell-cell contacts is of central importance in understanding the morphogenesis, architecture, and physiology of vertebrate organs, as well as the mechanisms underlying the pathogenesis of human disease. In epithelia, cell-cell junctions are essential to establish and maintain tissue integrity and barriers between tissue compartments, and they also play key roles in the transmission of signals to and from adjacent cells, and within tissues, to regulate proliferation and differentiation (1–4). The apical junctional complex includes two structurally and functionally distinct units, tight junctions (TJ)[3] and adherens junctions (AJ), whose canonical functions are paracellular barrier and intramembrane fence (TJ) (1) and cell-cell adhesion/mechanical tissue integrity (AJ), respectively (2, 3). AJ comprise cadherins and nectins as transmembrane adhesion molecules, both linked to the submembrane cortical cytoskeleton by cytoplasmic complexes of adaptor proteins: catenins (p120-catenin and β-catenin/α-catenin) for E-cadherin and afadin-ponsin for nectins (2, 5).

PLEKHA7 is a recently discovered cytoplasmic component of AJ, which was identified through its interaction with the AJ protein p120-catenin (6) and with the TJ/AJ protein paracingulin (CGNL1) (7–9). PLEKHA7 is specifically associated with the *zonula adhaerens* (ZA) (7), and it interacts with the microtubule-interacting protein nezha (CAMSAP3) to provide a molecular linkage between the cadherin-associated protein complex and the microtubule cytoskeleton (6). Genetic and genome-wide association studies have implicated PLEKHA7 in the regulation of cardiac contractility in a zebrafish model (10), in hypertension in human cohort studies (11–13) and in a rat model (14), and in primary angle closure glaucoma (15, 16). In addition, PLEKHA7 has recently been involved in the control of microRNA processing (17) and susceptibility to staphylococcal α-toxin (18). However, the molecular and cellular mechanisms through which PLEKHA7 is implicated in the above-mentioned diseases and in its cellular functions are still largely unknown.

To gain further insight into the biochemical basis for the functions of PLEKHA7, it is essential to identify and characterize new PLEKHA7 interacting partners. Toward this goal, we describe here the identification of PDZ domain-containing protein 11 (PDZD11) as a novel PLEKHA7 interactor. PDZD11 is recruited to AJ by PLEKHA7, contributing to the stabilization

* This work was supported in part by Swiss National Fund Grants 31003A103637 and 31003A116763 and the Swiss Cancer League Grant KFS-2813-08-2011 (to S. C.). The authors declare that they have no conflicts of interest with the contents of this article.
[1] Supported by the European Community's Seventh Framework Programme Grant FP7/2007-2013 under Grant Agreement 241548 (MitoSys Project).
[2] To whom correspondence should be addressed: Dept. of Cell Biology, 30 Quai Ernest Ansermet, 1211-4 Geneva, Switzerland. Tel.: 41-22-3796182; Fax: 41-22-3796868; E-mail: sandra.citi@unige.ch.

[3] The abbreviations used are: TJ, tight junction; AJ, adherens junction; Caco-2, colorectal carcinoma cell line-2; CFP, cyan fluorescent protein; mCCD, mouse kidney collecting duct; meEC, mouse embryonic aorta endothelial cell; MDCK, Madin-Darby canine kidney; PDZ, Psd95-Dlg1-ZO-1 domain; PDZD11, PDZ domain containing protein 11; PLA, proximity ligation assay; PLEKHA7, pleckstrin homology domain-containing family A member 7; Sf, *Spodoptera frugiperda*; ZA, *zonula adhaerens*; ZO-1, zonula occludens-1; IB, immunoblot; IF, immunofluorescence; PH, pleckstrin homology; qRT, quantitative RT.

of nectins at AJ and ensuring efficient early steps of junction assembly.

## Experimental Procedures

*Antibodies and Plasmids*—Antibodies are annotated below with information on species-antigen and dilution for either immunoblotting (IB) or immunofluorescence (IF) (using fixation with methanol unless otherwise stated), or proximity ligation assay (PLA). The following are used: rabbit PDZD11 (immune and preimmune r29958, 1:1500 IB, 1:50 IF); mouse β-tubulin (1:1000 IB, Zymed Laboratories Inc., catalog no. 32-2500); mouse Myc (9E10 hybridoma culture supernatant, 1:2 IB); rabbit and guinea pig PLEKHA7 (1:10,000 IB, 1:1000 IF, in-house r30388, gp2737, these latter raised against GST fusion proteins of canine PLEKHA7 residues 936–1237 and 611–809, respectively); mouse PLEKHA7 (378F1, 1:10 PLA (7)); mouse His (Invitrogen, catalog no. 37-2900, 1:1500 IB); mouse HA (1:1000 IB, Zymed Laboratories Inc., catalog no. 32-6700); rabbit cingulin (1:5000 IF, in-house C532 (19)); mouse cingulin (1:1000 IF, in-house 22BD5A1); rabbit paracingulin (1:10,000 IB, 1:500 IF, in-house 20893); rabbit α-catenin (1:4000 IB, 1:100 IF, Sigma, catalog no. c-2081); rabbit β-catenin (1:10,000 IB, 1:500 IF, Sigma, catalog no. C2206); mouse p120-catenin (1:2000 IB, 1:250 IF, 15D2 monoclonal, a kind gift from Prof. A. Reynolds); mouse E-cadherin (1:2000 IB, 1:2000 IF, BD610181); rabbit ZO-1 (1:1000 IB, Zymed Laboratories Inc., catalog no. 61-7300); rat ZO-1 (R40-76, 1:50 IF); mouse occludin (1:3000 IB, 1:300 IF, Zymed Laboratories Inc., catalog no. 33-1500); rabbit nectin-1 (Abcam, catalog no. AB66-985, 1:3000 IB, 1:500 PLA); rat nectin-3 (MBL-D084-3, 1:100 IF); rabbit nectin-3 (Abcam, catalog no. AB-63931, 1:4000 IB, 1:500 IF and PLA); rabbit afadin (Sigma, catalog no. A0224, 1:4000 IB, 1:600 IF); and VeriBlot secondary HRP-labeled antibodies for IP experiments (Abcam, catalog no. ab131366, 1:4000). The rabbit polyclonal anti-PDZD11 antiserum (r29958) was generated by immunization with recombinant full-length PDZD11 and obtained by affinity purification and thrombin protease digestion of GST-PDZD11 expressed in BL21DE3 bacteria. The full-length human PDZD11 sequence was obtained from Kazusa DNA Research Institute (clone number PF1KB8215) and amplified by PCR with appropriate oligonucleotides for subsequent subcloning. PDZD11 sequences (either full-length or truncated) were cloned into pGEX4T1 for bacterial expression as GST fusion proteins (EcoRI-XhoI). GFP-PDZD11-Myc was obtained in pcDNA3.1GFP-Myc (vector generated by NotI-ClaI digestion of the GFP-cingulin-Myc construct (20) (NotI-ClaI)). YFP- and Myc-tagged N-terminal, central, and C-terminal fragments of PLEKHA7 were described previously (21). GST fusions of smaller fragments of PLEKHA7 (WW, 1–162), WWPH(1–284), PH(120–300), and proline-rich + coiled-coil region (PCC, 500–844) were generated by PCR and subcloned into pGEX4T1. Other GST fusions of PLEKHA7 were described previously (7, 8). The internal WW and WF domains within the larger WW region (1–162) were subsequently identified and subcloned into pGEX4T1 to make three GST fusion constructs: W1 (WW, 1–53), W2 (WF, 43–98), and W1 + 2 (WW-WF, 1–98). Constructs of YFP-tagged (N-terminal) PLEKHA7 were generated in pTre2-Hyg as follows: full length (21), ΔPH (1–165 fused to 285–1121), and ΔWW (90–1121). The human nectin-1 (PVRL1) cDNA was obtained from Promega (pF1KB0475) and used by PCR amplification to subclone into the BamHI-NotI sites of pcDNA3.1Myc/His, with an N-terminal Myc sequence and a stop codon before the vector's Myc tag. The Myc-nectin1-Δ4, lacking the C-terminal PDZ-binding four residues (EWYV), was similarly generated by PCR and subcloned into pcDNA3.1Myc/His. All new constructs were verified by sequencing.

*Yeast Two-hybrid Screen and QUantitative BAC-Intera Ctomics (QUBIC)*—For the yeast two-hybrid screen, the full-length sequence of human *PLEKHA7* (residues 1–1121) was fused C-terminally to LexA in the pB27 vector. This construct was used to screen a human placenta library, in the presence of 0.5 mM 3-amino-1,2,4-triazole (Hybrigenics, Paris, France). A very high confidence interaction (PBS Score "A", based on the PIM predicted global biological score) was detected with 24 distinct clones of PDZD11, all of which contained the full-length coding sequence of PDZD11. In addition, a PBS score A was also obtained with six clones of the known interactor paracingulin (CGNL1) (8), whereas no PLEKHA7-interacting clones were detected with scores "B" (high confidence) or "C" (good confidence). For affinity purification of PLEKHA7 prior to mass spectrometry, a BAC clone harboring the mouse *Plekha7* gene (RP23-350A9, BACPAC Resources Center) was recombined with an N-terminal GFP BAC tagging cassette (NFLAP: GFP_PreScission_S-peptide_TEV_FLAG) (22). Precise incorporation of the tagging cassette was confirmed by PCR and sequencing. Next, the GFP-tagged BAC was isolated from bacteria using the NucleoBond PC100 kit (Macherey-Nagel, Germany), and HeLa Kyoto cells were transfected using Effectene (Qiagen) and cultured in DMEM selection media containing 400 μg/ml geneticin (G418, Invitrogen). The pool of HeLa cells stably expressing the tagged *Plekha7* transgene was analyzed by Western blot and immunofluorescence using an anti-GFP antibody (Roche Applied Science) to verify correct protein size and localization of the tagged transgene. Affinity purification and mass spectrometry were carried out as described (23). PDZD11 (Target ID Q5EBL8-2) and PLEKHA7 (Target ID Q6IQ23-2) were identified in the immunoprecipitate with the highest identical score of 10.296 (three peptides).

*Cell Culture, Preparation of Lysates, and Pharmacological Treatment*—We previously described culture conditions for MDCKII (Madin-Darby canine kidney), MDCK-Tet-Off epithelial cells (Clontech), Caco-2 (human intestinal carcinoma cells), mCCD (mouse kidney collecting duct, mpkCCD, clone N64, a kind gift of Prof. Eric Feraille, University of Geneva), and Sf21 insect cells (24–28). Culture conditions for human keratinocytes (HaCaT, a kind gift from Dr. L. Fontao, University of Geneva), human lung carcinoma cells (A427 and A459, a kind gift of Prof. M. Paggi, Istituto Regina Elena, Roma, Italy), mouse microvascular endothelioma cells (bEnd.3, a kind gift from Prof. B. Imhof, University of Geneva), and mouse aortic endothelial cells (meEC, a kind gift from Prof. B. Kwak, University of Geneva) will be described elsewhere. Total lysates were obtained in RIPA buffer (150 mM NaCl, 40 mM Tris-HCl, pH 7.5, 2 mM EDTA, 10% glycerol, 1% Triton X-100, 0,5% sodium deoxycholate, 0.2% SDS) supplemented with protease inhibitor

mixture (Roche Applied Science) from 10-cm dishes, followed by sonication (8 s at 66% amplitude with a Branson sonifier). To inhibit proteasome-mediated degradation, cells were treated with 25 μM MG132 (C2211, Sigma) for 8 h at 37 °C prior to lysis.

*Analysis of Dynamics of Junction Assembly by Calcium Switch*—A modification of the classical protocol (29) was used here, because mCCD cells undergo complete junction disassembly upon removal of extracellular calcium much more rapidly than MDCK cells. mCCD cells (300,000 cells inoculated on each round coverslip in 24-well plates 24 h earlier) were rinsed twice with PBS and incubated for 30 min in S-MEM low calcium medium (Gibco catalog no. 11380-052), containing 10 mM Hepes, pH 7.4, 1× non-essential amino acids, 5% FBS, 2 mM L-glutamine, 2 μM EGTA, and 1× penicillin/streptomycin, to disassemble junctions. To initiate junction assembly, the S-MEM medium was replaced with normal medium, and cells were fixed for immunofluorescent labeling at 15 and 30 min and 1 and 4 h after the switch. Junctional assembly of E-cadherin and cingulin was evaluated by immunofluorescence as described below.

*Generation of Knock-out (KO) mCCD Cells by CRISPR/Cas9 Genome Editing*—A construct for the CRISPR/Cas9-mediated knock-out (KO) of PDZD11 KO in mouse mCCD cells was generated by cloning a guide-RNA targeting exon-1 of the mouse *Pdzd11* gene (sequence: GCCGGCCTATGAAAACCCTC) into the BbsI site of px458 CRISPR plasmid (Addgene catalog no. 48138, containing GFP). Cells were transfected by Lipofectamine2000, and isolated clones were obtained 2 days later by fluorescence-activated cell sorting (using a Beckman Coulter MoFlo Astrios sorter, Flow Cytometry Service, University of Geneva Medical School). Single PDZD11-KO clones were screened by immunoblotting, and the genomic sequence of the *Pdzd11* locus was determined in distinct KO clones by PCR amplification and subcloning of a fragment spanning a 1-kb region, from the 5′-untranslated region of the *Pdzd11* gene to exon-2. Clone 1B2 showed the insertion of a G in both alleles (resulting sequence: GCCGGGCCTATGAAAACCCTC). Clone 2C7 showed a 2-bp deletion in allele 1 (G-GGCCTATGAAAACCCTC) and a 164-bp insertion in allele 2 (GCC-164 bp-GGCCTATGAAAACCCTC). Clone 1C8 showed a 2-bp deletion in allele 1 (G-GGCCTATGAAAACCCTC) and a 1-bp insertion in allele 2 (GCCGGGCCTATGAAAACCCTC). Rescue clones were obtained by expression of either GFP or GFP-tagged PDZD11 (cloned in pTre-2Hyg), and selection of clones was made in hygromycin-containing medium. The three clones behaved similarly, but only data from one clone (2C7) are shown in Figs. 4 and 6 for the sake of space. The generation of PLEKHA7-KO mCCD cells by CRISPR-mediated genome editing, the generation of rescue clones, and their full characterization will be described elsewhere.[4] Transfection was carried out using either Lipofectamine 2000 (Invitrogen) or the calcium phosphate method (for HEK293T cells).

*Immunofluorescence Microscopy, Immunohistochemistry, and Proximity Ligation Assay*—Conventional fixation of cells for labeling of junctional proteins was with methanol (10 min at −20 °C), and incubations with antibodies were for 30 min at 37 °C. To detect cytoplasmic GFP in PLEKHA7-KO cells, cells were fixed with Triton X-100 and paraformaldehyde (26). Immunohistochemistry was carried out as described previously (7). Proximity ligation assay (Sigma, catalog no. DUO92101) was carried out according to the manufacturer's instructions, using rabbit anti-nectin1/3 and mouse anti-PLEKHA7. Coverslips were mounted with Vectashield (Reactolab) and imaged with a Zeiss LSM700 confocal microscope, equipped with ×63, 1.3NA objective (Zeiss LSM software). LSM 8-bit files were converted to TIFF files separately for each channel using ImageJ software and linearly adjusted and cropped using Adobe Photoshop. Quantification of immunofluorescent junctional labeling for nectin-3 was carried out with ImageJ software, as described previously (8), using either E-cadherin or cingulin as an internal reference standard for junctional labeling (E-cadherin is not affected by PDZD11-KO, and cingulin is not affected by PLEKHA7-KO). Quantification of junction assembly during the calcium switch was carried out by drawing the outline of the cell periphery of 20 cells/field (three fields for each sample) (each cell was identified by DAPI-labeled nuclei), and by measuring the length of the regions of cell-cell contact that were labeled by either anti-E-cadherin or anti-cingulin antibodies. The percentage of junction assembly was obtained by ratioing the labeled lengths over the total calculated lengths of the cell peripheries.

*Immunoprecipitation, GST Pulldown, and Immunoblotting*—Immunoprecipitation of endogenous proteins from Caco2, mCCD, and meEC cells was carried out by rinsing cells with cold PBS and incubating them in 0.5 ml (coIP) of buffer (150 mM NaCl, 20 mM Tris-HCl, pH 7.5, 1% Nonidet P-40, 1 mM EDTA, 5 mg/ml antipain, 5 mg/ml leupeptin, 5 mg/ml pepstatin, 1 mM PMSF) for 10 min at 4 °C. After sonication (8 s at 40% power, Branson sonifier), the lysate was centrifuged for 15 min at 13,000 rpm. The supernatant was kept (cytoskeleton-soluble fraction). The pellet (cytoskeleton-insoluble fraction) was resuspended in 50 μl of SDS-buffer (1% SDS, 10 mM Tris-HCl, pH 7.5, 2 mM EDTA, 0.5 mM DTT, 0.5 mM PMSF), sonicated 2 s at 10% power, incubated at 100 °C for 5 min, clarified by centrifugation, brought to a volume of 0.5 ml with co-IP buffer, and mixed with the cytoskeleton-soluble fraction to make a "total" IP lysate. Dynabeads protein-G or protein-A (Invitrogen) (20 μl) were coupled to antibodies (either 2 μl of serum or 2 μg of purified antibody) at 4 °C for 90 min, washed with PBS containing 5% bovine serum albumin and 1% Nonidet P-40, and incubated with 0.1–0.3 ml of total IP lysate for 16 h at 4 °C. After washing three times with coIP buffer, beads were incubated in 20 μl of SDS sample buffer at 100 °C for 5 min, and between 5 and 15 μl of eluate were loaded on SDS gels (12% polyacrylamide for PDZD11 and 8% for PLEKHA7). SDS-PAGE and immunoblotting were carried out as described previously (21, 27). Protein loadings were normalized by immunoblotting with anti-tubulin antibody. Detection of proteins after Western blotting was performed by Odyssey Imager (LI-COR). Quantification of nectin-1 and nectin-3 protein levels by immunoblotting in normalized samples was carried out using ImageJ software analysis of scanned blots. Sf21 cells expressing His-tagged PLEKHA7 were lysed in LBT buffer (150 mM NaCl, 20 mM

[4] J. Shah, D. Guerrera, and S. Citi, unpublished results.

Tris-HCl, 5 mM EDTA, 1% Triton X-100, 5 mg/ml antipain, 5 mg/ml leupeptin, 5 mg/ml pepstatin, 1 mM PMSF), sonicated four times for 30 s at 30% power and centrifuged for 20 min at 13,000 rpm (8). Purification of GST fusion proteins and GST pulldowns with full-length His-tagged PLEKHA7 expressed in baculovirus-infected insect cells was performed as described previously (24, 25).

*RT-PCR*—mRNA levels for nectin-1 and nectin-3 in PDZD11-KO and rescue clones were measured by qRT-PCR, as determined previously (28), using GAPDH as an internal reference. The primers were as follows: nectin-1, forward 5′-TGCACTGTAGCTTTGCCAAC-3′ and reverse 5′-ATGTACATGCCCTCGTCCTC-3′; nectin-3, forward 5′-TTGCCCTTTCCTTTGTCAAC-3′ and reverse 5′-GCATGTCTGATGGTGGAATG-3′.

*Data Analysis*—All experiments were carried out at least in triplicate, and similar results were obtained when using distinct clones of either PLEKHA7-KO or PDZD11-KO cells. For immunoblots and immunofluorescence data, one representative example out of three independent experiments is shown. Statistical significance of quantitative data was determined by Student's *t* test.

## Results

*PDZ Domain-containing Protein 11 Is a Novel Interactor of PLEKHA7*—We sought to identify novel interactors of PLEKHA7 by yeast two-hybrid screen and by mass spectrometry analysis of affinity-purified PLEKHA7 immunoprecipitates. Both approaches identified PDZD11, also known as PISP (plasma membrane calcium ATPase-interacting single-PDZ protein) or AIPP1 (ATPase-interacting PDZ protein) (30–32) as the highest confidence interactor of PLEKHA7. We generated a rabbit polyclonal antiserum against PDZD11, which specifically labeled a polypeptide of 17 kDa in lysates of MDCK, mCCD, human keratinocytes (HaCaT), human lung carcinoma cells (A427 and A549), mouse endothelial cells (bEnd.3, meEC), human colon carcinoma cells (Caco-2), and mouse kidney tissue, consistent with the predicted size of PDZD11 (Fig. 1, *A* and *B*). The antiserum specifically immunoprecipitated exogenously expressed PDZD11, containing N-terminal GFP and C-terminal Myc tags, from MDCK cell lysates (Fig. 1*C*). To validate the findings of the two-hybrid screen and mass spectrometry analysis, we explored the PLEKHA7-PDZD11 interaction by co-immunoprecipitation and GST-pulldown experiments. First, PDZD11 was detected in PLEKHA7 immunoprecipitates from lysates of endothelial (aorta, meEC) and epithelial (kidney, mCCD) cells (Fig. 1*D*). Second, PLEKHA7 was detected in PDZD11 immunoprecipitates from lysates of Caco2 colon epithelial cells (Fig. 1*E*). Third, bacterially expressed full-length PDZD11 interacted with full-length His-tagged PLEKHA7, isolated from insect cells (Fig. 1*F*). Taken together, these results demonstrate that PDZD11 is expressed in epithelial and endothelial cells and tissues, where it forms a complex and directly interacts with PLEKHA7.

*The First WW Domain of PLEKHA7 Interacts with the N-terminal 44 Residues of PDZD11 (P7-ID)*—To identify the sequences involved in PLEKHA7-PDZD11 interaction, we generated mutated constructs of the proteins to use in GST-pull-down assays. PLEKHA7 comprises WW and PH domains in its N-terminal half and coiled-coil and proline-rich domains in its C-terminal half (Fig. 2*A*). PLEKHA7 prey (N- and C-terminal

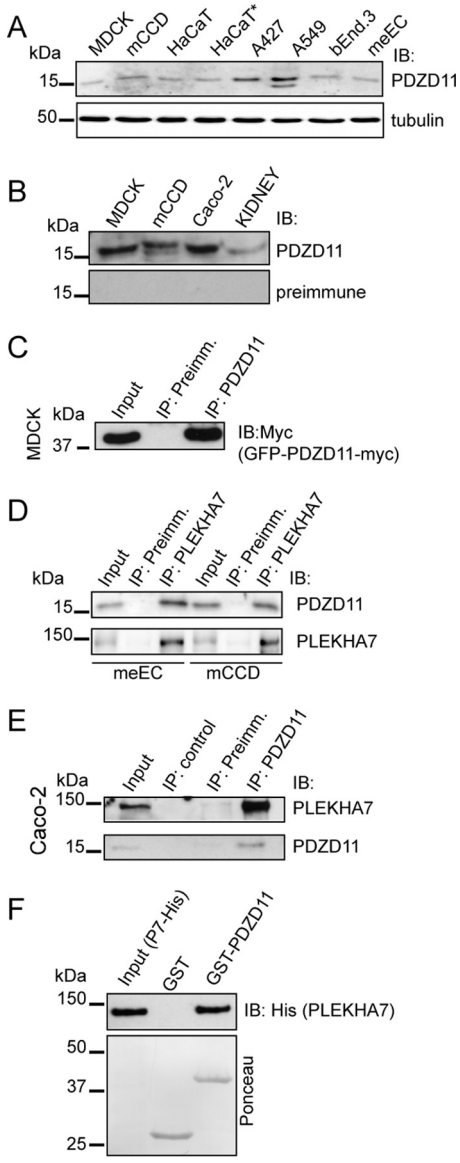


FIGURE 1. **PLEKHA7 forms a complex and interacts directly with PDZD11.** *A–C,* characterization of a rabbit anti-PDZD11 antiserum by immunoblotting analysis of the following. *A,* lysates of kidney epithelial (MDCK, mCCD) cells, human keratinocytes (HaCaT), human lung carcinoma cells (A427, A549), and mouse endothelial cells (bEnd.3, meEC) (tubulin levels for normalization of total protein loading is shown below). The *asterisk* near one lane of HaCaT lysates indicates overconfluent cells. *B,* lysates of MDCK, mCCD, and human colon carcinoma cells (Caco2) and mouse kidney with immune and pre-immune anti-PDZD11 antisera. *C,* immunoprecipitates of exogenously expressed GFP-PDZD11-Myc (in MDCK cells) with immune and pre-immune anti-PDZD11 antiserum. *D–F,* PDZD11 forms a complex and interacts directly with PLEKHA7. *D, top panel,* PDZD11 is detected by immunoblotting in PLEKHA7 immunoprecipitates from lysates of both meEC (*left lanes*) and mCCD cells (*right lanes*). *Bottom panel,* detection of PLEKHA7 in PLEKHA7 immunoprecipitate. Immunoprecipitates with pre-immune only are also shown. *E, top panel,* PLEKHA7 is detected in PDZD11 immunoprecipitates from lysates of Caco-2 cells. *Bottom panel,* detection of PDZD11 in the PDZD11 immunoprecipitate. Immunoprecipitates with pre-immune and immune sera and beads alone (control) are shown. *F,* GST pulldowns of lysates of insect cells expressing full-length His-tagged PLEKHA7, using either GST or GST-PDZD11 as baits, using anti-His antibodies. *Numbers* on the left indicate size (kDa) and migration of prestained markers. *Input lanes* = 0.1 of lysate volume used for immunoprecipitate.

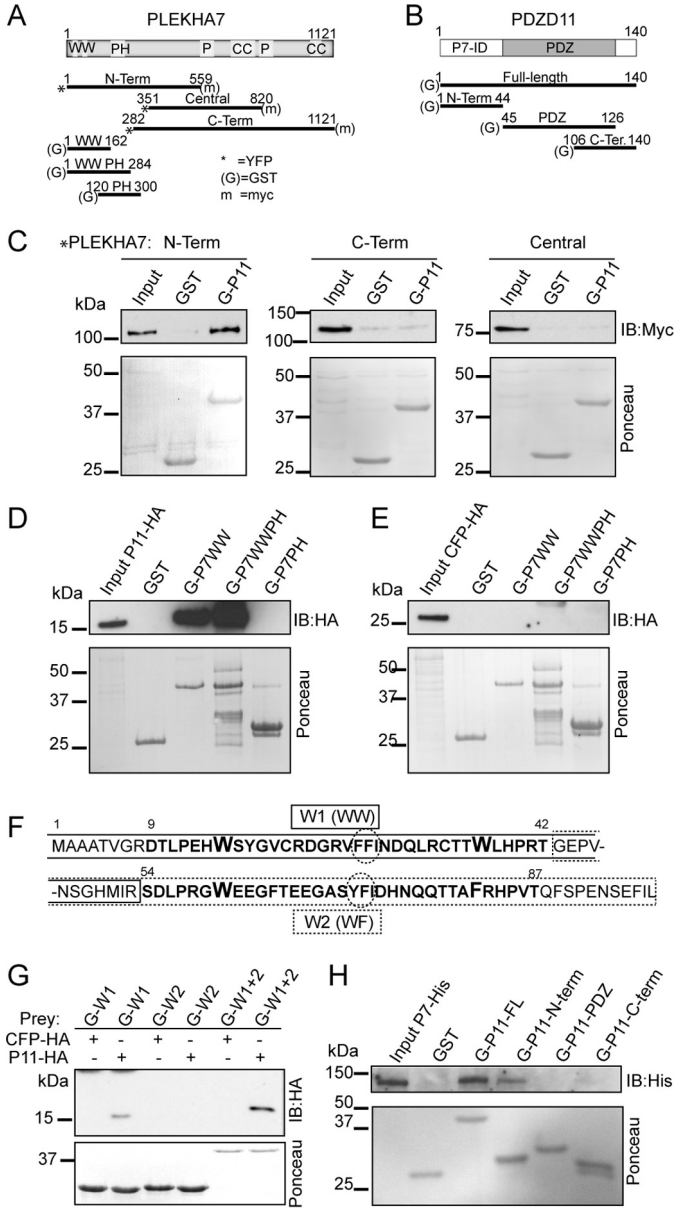


FIGURE 2. **The first WW domain of PLEKHA7 interacts with the N-terminal 44 residues of PDZD11.** *A* and *B,* schematic diagrams of PLEKHA7 (*A*) and PDZD11 (*B*), showing structural domains and amino acid boundaries of full-length and truncated constructs used in GST-pulldown assays. Note: the schemes of PLEKHA7 and PDZD11 are not size-scaled. *, *m,* and *G* indicate GFP, Myc, and GST tags, respectively. *C,* immunoblot analysis, using anti-Myc antibodies, of GST pulldowns of lysates of MDCK cells expressing GFP-tagged constructs of PLEKHA7 (as schematically shown in *A*) (21) and either GST or GST-PDZD11 as baits. *D,* immunoblot analysis, using anti-HA antibodies, of GST pulldowns using GST (*G*-) fused to different domains (WW, WW and PH, and PH domain alone) of PLEKHA7 (see *A* for scheme) as baits and either HA-tagged PDZD11 (P11-HA) (*D*) or HA-tagged CFP (CFP-HA) (*E*) as preys. *F,* amino acid sequence of the first 98 residues of human PLEKHA7, and highlighted in *bold* are the W1 domain (WW domain, Trp = W residues are highlighted in larger size) and the W2 domain ("WF" domain, Trp = W and Phe = F residues are highlighted in larger size). The *boxes* show residues included in W1 construct (*continuous line,* residues 1–53) and in W2 construct (*dotted line,* residues 43–98). The cluster of aromatic amino acid at the center of each WW domain is highlighted by a *dotted circle*. *G,* immunoblot analysis, using anti-HA antibodies, of GST pulldowns using GST (*G*) fused either to the W1 sequence or the W2 sequence, or both (*W1 + 2*) (see *F* for residues), and either HA-tagged CFP (*CFP-HA*) or HA-tagged PDZD11 (*P11-HA*) as preys (+ or − indicate which prey is used in each lane). *H,* immunoblot analysis, using anti-His antibodies, of GST pulldowns of lysates of Sf21 insect cells expressing His-tagged full-length PLEKHA7 using GST fusion constructs of PDZD11, as schematically shown in *B*. Images of Ponceau-S-stained blots shows the amounts of recombinant proteins used as baits. Numbers on the *left* indicate size (kDa) and migration of prestained markers.

and central regions) containing N-terminal YFP and C-terminal Myc tags were obtained from lysates of stably transfected MDCK cell lines (Fig. 2, *A* and *C*) (21). Another PLEKHA7 prey consisted of His-tagged full-length PLEKHA7 obtained from lysates of insect cells infected with baculovirus (Fig. 2*H*) (8). PDZD11 consists of a 44-residue N-terminal peptide, followed by a 81-residue PDZ domain and a 14-residue C-terminal peptide (Fig. 2*B*). PDZD11 baits consisted of GST fused N-terminally to 1) full-length sequence, 2) N-terminal peptide, 3) PDZ domain, 4) the 21 C-terminal residues of the PDZ domain, followed by the 14-residue C-terminal peptide (Fig. 2, *B* and *H*). Immunoblot analysis of GST pulldowns showed that full-length PDZD11 interacts with the YFP-tagged N-terminal region of PLEKHA7, but not with C-terminal or central domains of PLEKHA7 (Fig. 2*C*), indicating that the PDZD11-interacting region in PLEKHA7 lies within residues 1–282 of PLEKHA7. This region includes Trp-Trp (WW) and PH domains (Fig. 2*A*). GST fusions of these domains, together or separately, were generated to prepare baits for pulldown assays (Fig. 2*A*). Pulldown experiments using HA-tagged PDZD11 as a prey showed that the N-terminal fragment of PLEKHA7 (residues 1–162) comprising the WW domains, either alone or in combination with the PH domain, but not the PH domain alone, specifically binds to PDZD11 (Fig. 2, *D* and *E,* for control pulldowns with CFP-HA). PLEKHA7 actually contains two WW domains (33). The first contains the canonical Trp-Trp signature, and the second contains a Trp and a Phe residue; the two domains are separated by a spacer region of 11 residues. We generated GST fusions comprising either the first WW (W1, Fig. 2*F*) or the second (W2, Fig. 2*F*), or both (W1 + 2), and we examined their interaction with full-length PDZD11 by pulldown assays (Fig. 2*G*). Only the first, but not the second, WW domain could interact, when isolated, with PDZD11. However, a stronger interaction was detected when both W1 and W2 domains were present in the fusion protein (Fig. 2*G*). Finally, GST fusion proteins were generated to map the region of PDZD11 involved in interaction with PLEKHA7 (Fig. 2, *B* and *H*). GST fusions of full-length PDZD11 and N-terminal peptide interacted with the full-length His-tagged PLEKHA7 in insect cell lysates, but no interaction of PLEKHA7 was detected with GST fusions of either the PDZ domain of PDZD11 or the C-terminal construct (Fig. 2*H*). Because its sequence is unique, and it binds specifically to PLEKHA7, we propose to name the 44-residue N-terminal sequence of PDZD11 P7-ID (PLEKHA7 interacting domain).

*PLEKHA7 Recruits PDZD11 to Epithelial Adherens Junctions*—Because PLEKHA7 is accumulated at the *zonula adhaerens* (7), the interaction between PLEKHA7 and PDZD11 predicts that PDZD11 should also be localized at AJ in epithelial cells and tissues. To test this, we first labeled epithelial cell lines and kidney tissue by immunofluorescence with the anti-PDZD11 antiserum. Junctional labeling for PDZD11 that co-localized with TJ and AJ markers was detected in MDCK, A427, meEC, and additional epithelial cell types and kidney tissue (Fig. 3*A*,

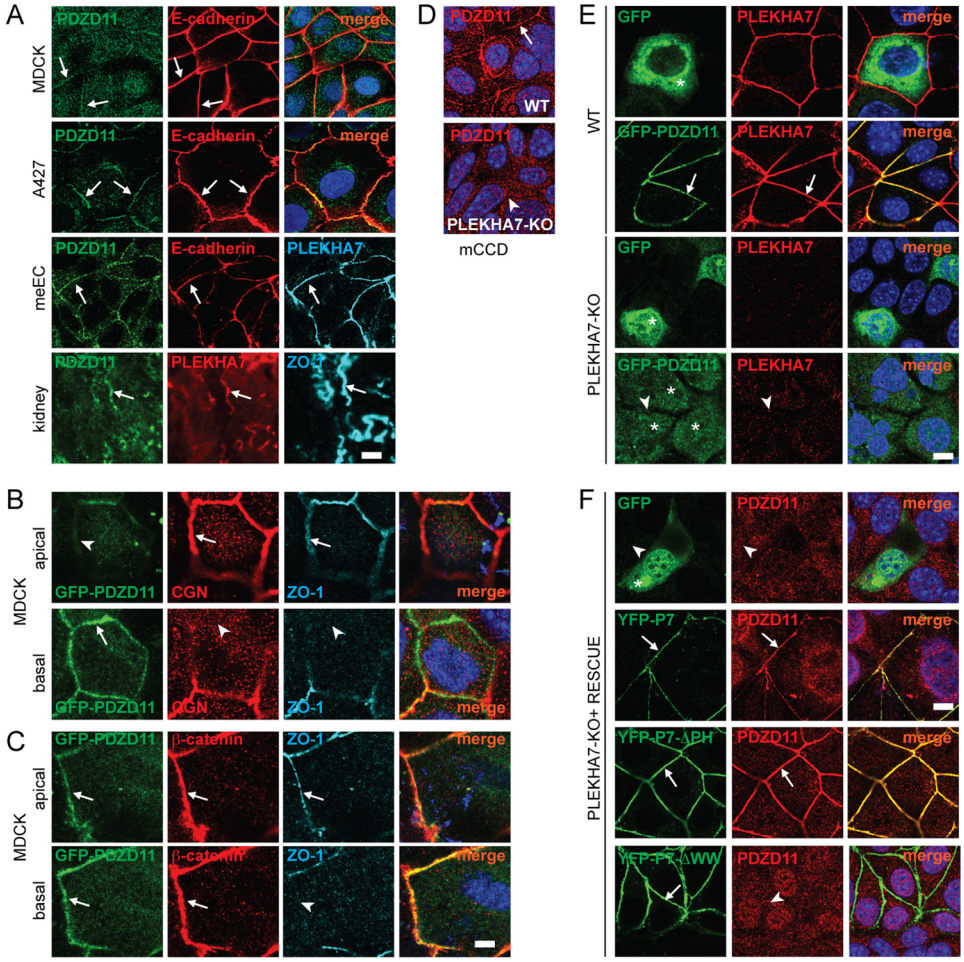


FIGURE 3. **PLEKHA7 recruits PDZD11 to adherens junctions.** *A,* PDZD11 is localized at cell-cell junctions in epithelial and endothelial cells and tissues as follows: immunofluorescent localization of endogenous PDZD11 at junctions of MDCK cells, A427 cells, meEC cells, and frozen sections of mouse kidney, using the anti-PDZD11 antiserum. MDCK and A427 cells were double-labeled with E-cadherin antibodies, and meEC cells were triple-labeled with E-cadherin and PLEKHA7 antibodies, to identify adherens junctions. The kidney section was triple-labeled with PLEKHA7 and ZO-1 to identify zonular junctions. *B* and *C,* exogenous PDZD11 co-localizes with AJ markers as follows: immunofluorescence analysis of serial z-sections of MDCK cells expressing exogenous GFP-tagged PDZD11, and double-stained for either cingulin and ZO-1 (*B*) or for β-catenin (*beta-cat*) and ZO-1 (*C*), as markers of TJ (cingulin and ZO-1) or AJ (β-catenin). *D–F,* PLEKHA7 recruits PDZD11 to epithelial AJ. *D,* immunofluorescence analysis of either WT or PLEKHA7-KO (P7-KO) mCCD cells, using anti-PDZD11 antiserum. Three distinct clones of PLEKHA7-KO cells gave identical results with regard to loss of junctional PDZD11. *E,* immunofluorescence analysis of either WT or PLEKHA7-KO mCCD cells, transiently expressing either GFP or GFP-PDZD11, using anti-PLEKHA7 antibodies (GFP fluorescence was visualized directly). *F,* immunofluorescence analysis of PLEKHA7-KO mCCD cells, transiently expressing either GFP or YFP-PLEKHA7 or YFP-PLEKHA7 with an internal deletion of the PH domain (YFP-P7-ΔPH), or PLEKHA7 with an N-terminal truncation of the WW domains (*YFP-P7-ΔWW*), using anti-PDZD11 antibodies (YFP green fluorescence was visualized directly). Merge images show nuclei in *blue* (DAPI). *Arrows* indicate junctional labeling, and *arrowheads* indicate lack of junctional labeling, and *asterisks* indicate cytoplasmic labeling. *Scale bar,* 10 μm (*A, B,* and *D–F*) and 5 μm (*C*).

data not shown). To establish more clearly the localization of PDZD11, we imaged serial apico-basal confocal z-sections of MDCK cells expressing GFP-tagged PDZD11 and double-labeled with markers of either TJ (cingulin and ZO-1) or AJ (β-catenin) (Fig. 3, *B* and *C*). Immunofluorescence analysis showed that GFP-PDZD11 labeling only partially overlapped with endogenous cingulin and ZO-1 labeling along apicolateral junctions (*arrow* and *arrowhead* in Fig. 3*B*), whereas it overlapped more precisely with endogenous labeling for junctional β-catenin (*arrows* in Fig. 3*C*). This is very similar to the localization of endogenous and exogenous PLEKHA7 in epithelial cells (8, 21). Next, we asked whether PDZD11 is recruited to adherens junctions by PLEKHA7, by examining the localization of endogenous PDZD11 in either wild-type (WT) mCCD or in cells where both PLEKHA7 alleles were targeted by CRISPR-mediated gene disruption, and which do not express PLEKHA7 (PLEKHA7-KO) (Fig. 3, *D–F*). Junctional labeling for PDZD11 was detected in WT cells but not in PLEKHA7-KO cells (*arrow* and *arrowhead* in Fig. 3*D*, respectively). Next, we transiently expressed either GFP or GFP-tagged PDZD11 in either WT or PLEKHA7-KO mCCD cells (Fig. 3*E*). Labeling for the GFP control protein was detected diffusely in the cytoplasm both in WT and in PLEKHA7-KO cells (*asterisks* in Fig. 3*E*). Importantly, exogenous GFP-tagged PDZD11 was detected exclusively at junctions in WT cells (*arrows* in Fig. 3*E, WT*), where it co-localized precisely with PLEKHA7. In contrast, exogenous GFP-tagged PDZD11 was localized exclusively in the cytoplasm in PLEKHA7-KO cells (*asterisks* and *arrowheads* in Fig. 3*E,* PLEKHA7-KO). PLEKHA7-KO mCCD cells form junctions similar to WT cells, as determined by labeling with most markers of TJ and AJ, and establish a normal TJ barrier.[4] This indicates that the lack of association of exogenous PDZD11 with

junctions in PLEKHA7-KO cells is specifically due to the absence of PLEKHA7, rather than to secondary effects on other components of zonular junctions. To confirm the role of PLEKHA7 in recruiting PDZD11, we carried out a rescue experiment by re-expressing either GFP- or YFP-tagged PLEKHA7 and either WT or mutant in PLEKHA7-KO mCCD cells (Fig. 3*F*). Immunofluorescence analysis showed that the junctional localization of PDZD11 was rescued in PLEKHA7-KO cells, upon exogenous expression of either full-length PLEKHA7 (*arrows* in Fig. 3*F*, *YFP-PLEKHA7*) or PLEKHA7 lacking the PH domain (*arrows* in Fig. 3*F*, *YFP-P7-ΔPH*), but not upon expression of PLEKHA7 lacking the N-terminal WW domains (*arrowhead* in Fig. 3*F*, *YFP-P7-ΔWW*). In addition, junctional labeling for endogenous PDZD11 was increased in WT cells that overexpressed exogenous PLEKHA7 (data not shown), supporting the idea that the accumulation of PDZD11 at junctions is promoted by PLEKHA7. Taken together, these results demonstrate that PLEKHA7 recruits PDZD11 to epithelial junctions through its WW domain-containing N-terminal region.

*PDZD11 Is Required to Stabilize Nectin-1 and Nectin-3 at Epithelial Adherens Junctions*—To determine the role of PDZD11 in the molecular architecture of epithelial junctions, we analyzed the localization and expression of zonular (ZO-1, afadin, paracingulin, cingulin, and PLEKHA7) and zonular/lateral (occludin, E-cadherin, α-catenin, β-catenin, and p120-catenin) junctional markers in cells where both alleles of *Pdzd11* were inactivated by CRISPR-mediated genome editing. When mixed cultures of WT and PDZD11-KO cells were analyzed by immunofluorescence (to identify better the differences between WT and KO cells in the same field), the localization of PLEKHA7 and ZO-1 was not detectably altered in PDZD11-KO cells, when compared with neighboring WT cells (Fig. 4*A*, *top row*). No labeling for PDZD11 was detected in KO cells by either immunofluorescence (Fig. 4*A*) or immunoblotting (Fig. 4*B*), confirming the specificity of the anti-PDZD11 antiserum. The immunofluorescent localization (Fig. 4*A* and data not shown) and the levels of expression (Fig. 4*B*), not only of PLEKHA7 but also of the other zonular and zonular/lateral tight and adherens junction markers (E-cadherin, cingulin, occludin, afadin, p120-catenin, α-catenin, β-catenin, and paracingulin), were not detectably altered in confluent PDZD11-KO cells (Fig. 4, *A* and *B*). Next, we examined the localization and expression of nectins, Ig-like cell adhesion molecules localized at adherens junctions, that display PDZ-binding motifs at their C-terminal cytoplasmic tail (34, 35). In three distinct PDZD11-KO clones, we observed a decrease in junctional labeling for nectin-3 (Fig. 4, *C, top row*, showing only clone 2C7, and quantification in *D*). The decreased junctional labeling for nectin-3 in PDZD11-KO cells was rescued by re-expression of GFP-tagged PDZD11 but not of GFP (*double arrows* in Fig. 4*C*, *2nd row*). By immunoblotting, we observed decreased levels of expression of both nectin-1 and nectin-3 in PDZD11-KO cells (Fig. 4*E* and quantification in *F*), with no significant changes in nectin mRNA levels, as determined by qRT-PCR (Fig. 4*G*). Nectin-1 and nectin-3 protein levels in PDZD11-KO cells were rescued by re-expression of GFP-tagged PDZD11, but not of GFP alone (Fig. 4*E* and quantifications in *F*). To ask whether the decreased levels of nectin-1 and nectin-3 in PDZD11 KO cells were due to decreased stability, *e.g.* increased degradation, we treated either WT or KO cells with the proteasome inhibitor MG132 (Fig. 4*H* and *I* for quantification). Immunoblot analysis showed that normal levels of nectin expression were rescued in PDZD11 KO cells upon treatment with MG132 (Fig. 4, *H* and *I*), revealing a proteasome-dependent degradation of nectin. Next, we tested the hypothesis that the junctional localization and expression of nectin-1 and nectin-3 should also be altered in PLEKHA7-KO cells, because PLEKHA7 recruits PDZD11 to junctions. Immunofluorescence (Fig. 4*C*, *3rd* and *4th rows*) and immunoblotting (Fig. 4*J* and quantifications in *K*) analyses showed that PLEKHA7-KO cells phenocopied PDZD11KO cells, because junctional nectin-3 labeling and nectin-1 and nectin-3 protein levels were reduced in PLEKHA7-KO cells and rescued upon re-expression of PLEKHA7. These data demonstrate that although PDZD11 is not required to maintain the molecular organization of either TJ or the E-cadherin-associated complex at steady state, the PLEKHA7-PDZD11 complex is required for the efficient recruitment and stabilization of nectins at AJ.

*PDZD11 Binds Directly to Nectin-1*—To examine the molecular basis for the regulation of nectin junctional accumulation and stability by the PDZD11-PLEKHA7 complex, we studied the physical interaction of PDZD11 and PLEKHA7 with nectins. Immunoprecipitation experiments show that endogenous nectin-1 and nectin-3 immunoprecipitate PDZD11 (Fig. 5*A*). In contrast, we were unable to detect PLEKHA7 in nectin immunoprecipitates. To determine whether PDZD11 or PLEKHA7 interacts directly with nectins, GST fusion constructs of PDZD11 and PLEKHA7 were used as baits to bind Myc-tagged nectin, expressed in HEK293T cells. Immunoblot analysis showed that full-length nectin-1 is detected specifically in GST pulldowns of PDZD11 but not in GST pulldown using fragments of PLEKHA7 from the N-terminal, central, or C-terminal domains (Fig. 5*B*). Next, we asked whether the interaction between nectin-1 and PDZD11 depends on the interaction between the PDZ domain of PDZD11 and the PDZ-binding motif of nectin-1. No binding to the PDZD11 GST fusion bait was observed when the four-residue PDZ-binding motif of nectin-1 was deleted (Myc-nectin1-Δ4 in Fig. 5*C*). Furthermore, only the PDZ fragment of PDZD11 could bind nectin-1 but not the N-terminal P7-ID nor the C-terminal fragments (Fig. 5*D*). Finally, we used the PLA to detect the physical association between PLEKHA7 and either nectin-1 or nectin-3. In both cases, a strong junctional accumulation of labeling was detected in WT cells (*double arrows* and *magnified insert* in Fig. 5*E*, *WT panels*). However, only background labeling was observed in PLEKHA7-KO cells (*arrowhead* and *magnified inset* in Fig. 5*E*, *PLEKHA7-KO panels*), demonstrating that the proximity between nectins and PLEKHA7 is specifically due to PLEKHA7. Importantly, in PDZD11 KO cells there was a strong reduction in junctional signal with respect to WT cells (*arrow* and *magnified inset* in Fig. 5*E*, *PDZD11-KO panels*). This indicates that PDZD11 is critical to ensure maximal physical proximity between PLEKHA7 and nectins and that residual association between nectins and PLEKHA7 may be indirect, through afadin. Taken together, the GST pulldown and PLA results demonstrate that a complex of PLEKHA7 and PDZD11 is required

for the efficient recruitment and stabilization of nectins at AJ, through the binding of the PDZ-binding motif of nectins to the PDZ domain of PDZD11.

*PDZD11 Is Required for the Efficient Early Assembly of Apical Junctions in the Calcium-switch Experimental Model*—To address the cellular functions of PDZD11, we hypothesized,

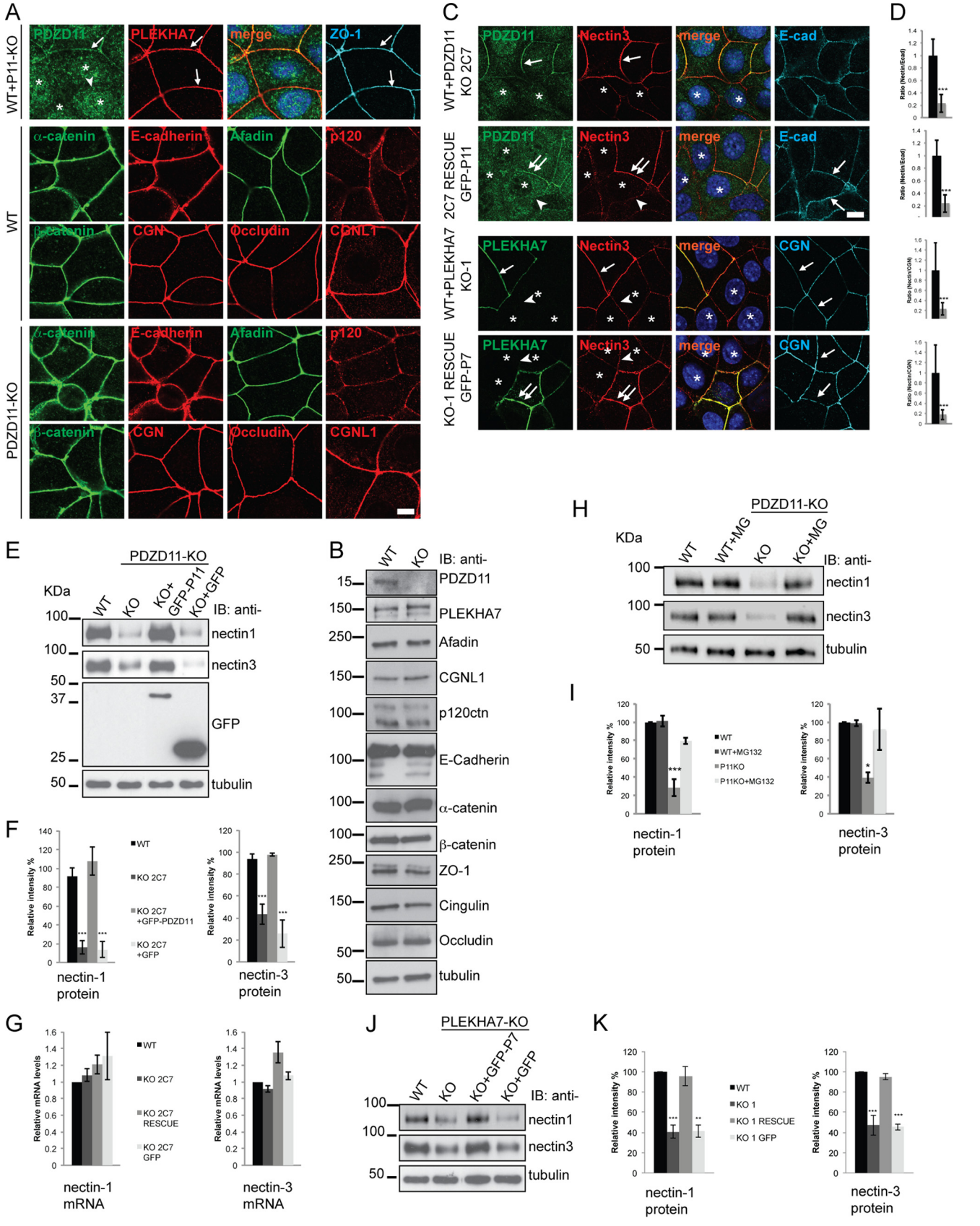

based on the effects of the PLEKHA7-PDZD11 complex on nectin junctional localization and stability, that we might detect a phenotype related to the function of nectins, which are implicated in early junction assembly (see under "Discussion") (5). Analysis of junctions at steady state showed that WT and PDZD11-KO cells are indistinguishable when examining a large number of markers (Fig. 4). Therefore, we examined the role of PDZD11 in the dynamic assembly of apical junctions, by using the calcium-switch protocol, which is the most commonly used experimental model to investigate the biogenesis of junctions in epithelial cells (29). Cells were immunofluorescently labeled with antibodies against cingulin (TJ marker) and E-cadherin (AJ marker) at different times after the start of junction assembly by the calcium switch (15 and 30 min and 1 and 4 h, Fig. 6, *A* and *D*). Junction assembly was scored by quantifying linear junctional labeling for each marker *versus* putative total junctional length (Fig. 6, *B, C, E,* and *F*). At 15 and 30 min after the calcium switch, WT cells showed 20 and 35% of junction assembly, respectively, corresponding to clearly identifiable segments of E-cadherin and cingulin labeling at the cell periphery (*arrows* in Fig. 6, *A, WT*, and quantifications in *B* and *C*). In contrast, in PDZD11 KO cells only 8 and 20% of junctions were assembled after 15 or 30 min, respectively, corresponding to fewer segments of the cell peripheries labeled by the cingulin and E-cadherin antibodies (*arrows* in Fig. 6, *A,* and quantifications in *B* and *C*). In PDZD11-KO cells, E-cadherin and cingulin labeling were detected mostly in a granular perinuclear pattern (*arrowheads* in Fig. 6*A*), suggesting an accumulation in endoplasmic reticulum/Golgi compartments. The differences between WT and PDZD11-KO cells were no longer observed at 1 and 4 h after the beginning of the calcium switch (WT and KO in Fig. 6*D* and quantifications in *E* and *F*). After 4 h, junctions were fully assembled (Fig. 6, *D* and *F*). The slight early delay in junction assembly observed in PDZD11-KO cells was specifically due to the lack of PDZD11 and not to clone-dependent variations, because the phenotype was rescued by the stable re-expression of GFP-PDZD11 but not by the re-expression GFP alone (*KO*+*GFP-PDZD11* and *KO*+*GFP* in Figs. 6, *A–C*, and see 4*E* for immunoblots of transgenes). Therefore, the absence of PDZD11 causes a slight delay in the very initial phases of junction assembly, but this delay is eventually overcome, allowing the formation of junctions with localization and expression of junctional proteins indistinguishable from that of WT cells.

## Discussion

Here, we identify PDZD11 as a new interactor of PLEKHA7, and we show that PDZD11 is recruited by PLEKHA7 to AJ, to promote the efficient junctional recruitment and stabilization of nectins and the efficient early phases of assembly of apical junctions in epithelial cells. These results uncover a new function for PLEKHA7, in organizing the junctional clustering of PDZ-interacting proteins, through PDZD11. They also show that PLEKHA7 stabilizes both major adhesion transmembrane proteins of adherens junctions (cadherins and nectins), through binding to components of the respective cytoplasmically associated complexes: p120-catenin/paracingulin for E-cadherin and PDZD11-afadin for nectins (Fig. 7).

Considering the potentially critical role of PLEKHA7 in major human pathologies, such as hypertension and glaucoma, it is essential to learn more about its molecular interactors and its cellular functions. Here, we report that two different types of screening technologies identify PDZD11 as the top hit among PLEKHA7 interactors, and we confirm the relevance of the PLEKHA7-PDZD11 interaction, as well as of the interaction

FIGURE 4. **PDZD11 and PLEKHA7 are required for the efficient recruitment and stabilization of nectins at adherens junctions.** *A,* PDZD11 is not required for the integrity of adherens and tight junctions. *Top panel,* immunofluorescence analysis of mixed cultures of wild-type (*WT*) and PDZD11 knock-out (*KO*) cells with antibodies against PDZD11 (rabbit, Alexa488), PLEKHA7 (guinea pig, Cy3), and ZO-1 (rat, Cy5). *Merge* images show nuclei labeled in *blue* (DAPI). *Arrows* indicate junctional labeling; *arrowheads* indicate lack of junctional labeling; *asterisks* indicate KO cells. *Bottom panels,* individual cultures (not mixed) of either WT or PDZD11-KO cells were immunofluorescently labeled with antibodies against E-cadherin, afadin, α-catenin, β-catenin, p120-catenin, cingulin, paracingulin, and occludin. *B,* immunoblot analysis of lysates of wild-type (*WT*) and PDZD11-KO (*KO*) mCCD cells, using antibodies against PDZD11, PLEKHA7, afadin, paracingulin, p120-catenin (p120), E-cadherin, α-catenin, β-catenin, ZO-1, cingulin, occludin, and tubulin (for loading control). *C,* PDZD11 and PLEKHA7 are required for the junctional accumulation of nectin-3. Immunofluorescence analysis of (*from top to bottom*): *1st row*: mixed cultures of WT cells + 2C7 PDZD11-KO clone to identify differences in neighboring WT *versus* KO cells; *2nd row*: mixed cultures of the PDZD11-KO clone (2C7) rescued with GFP together with cells of the same clone rescued with GFP-PDZD11: again, to compare directly nectin-3 labeling in mock-rescued cells (GFP) or in cells rescued with the GFP-PDZD11 construct. *3rd row*: mixed cultures of WT cells + PLEKHA7-KO clone 1 (KO-1); *4th row*: mixed cultures of the PLEKHA7-KO-1 clone rescued with GFP together with cells of the same clone rescued with GFP-PLEKHA7. Cells were labeled with antibodies against either PDZD11 (*1st* and *2nd rows*) or PLEKHA7 (*3rd* and *4th rows*) to identify WT and KO cells (or cells expressing exogenous GFP-PDZD11 or GFP-PLEKHA7 rescue), with antibodies against nectin-3 to examine nectin-3 accumulation, and with either E-cadherin (*E-cad*) (*1st* and *2nd rows*) or cingulin (*CGN*) (*3rd* and *4th rows*) to identify junctional regions. The same results were obtained with additional clonal lines of PDZD11-KO cells (1B2 and 1C8) and PLEKHA7 (KO-5 and KO-7) (data not shown). *Arrows* and *arrowheads* indicate normal or decreased junctional labeling, respectively; *double arrows* indicate increased junctional labeling in cells expressing either the GFP-PDZD11 or GFP-PLEKHA7 constructs; *asterisks* identify the nuclei of either KO cells (*1st* and *3rd row*) or KO cells rescued with GFP alone (*2nd* and *4th rows*), which is not visible in the cytoplasm, due to methanol fixation. *D, histograms* showing the quantification of junctional labeling for nectin-3 in the corresponding panels, expressed as a ratio between nectin-3 and either E-cadherin (*rows 1* and *2*) or cingulin (*rows 3* and *4*) labeling in junctions between WT cells (*black*) or between KO cells (*gray*). *E,* immunoblot analysis of nectin-1 and nectin-3 levels in lysates from WT cells and from the PDZD11 2C7 clonal line, either without or with re-expression of exogenous GFP-PDZD11 (GFP-P11) (or GFP, as a control) for rescue. Immunoblotting with anti-GFP is also shown, to detect expression of rescuing proteins. *F, histograms* showing the quantification (based on densitometric scan of blots) of relative protein levels for nectin-1 (*left*) or nectin-3 (*right*), by considering protein levels in WT clones (*black*) as 100% and expressing protein levels in KO 2C7 clone (*dark gray*), KO 2C7 clone + GFP-PDZD11 rescue (*light gray*), KO 2C7 clone + GFP rescue (*very light gray*) as percentages of WT. *G, histograms* showing levels of either nectin-1 mRNA (*left*) or nectin-3 mRNA (*right*) in WT, PDZD11-KO (clone 2C7), and rescued clonal lines, as determined by qRT-PCR. See *F* for labeling of columns. *H,* PDZD11 stabilizes nectins by preventing their proteasome-mediated degradation. Immunoblot analysis of nectin-1 and nectin-3 levels in lysates from either WT or PDZD11KO cells (clone 2C7), either untreated (WT, KO) or treated with the proteasome inhibitor MG132 (*WT*+*MG* and *KO*+*MG*). *I, histograms* showing the quantification of relative protein levels for nectin-1 (*left*) or nectin-3 (*right*), in either WT cells (*black* and *dark gray columns*) or PDZD11 KO clone 2C7 (*light* and *very light grays*), either without (*black light gray*) or with (*dark* and *very light gray*) treatment with MG132. *J,* immunoblot analysis of nectin-1 and nectin-3 levels in lysates from WT cells and from the PLEKHA7-KO-1 clonal line, either without or with re-expression of exogenous GFP-PLEKHA7 (GFP-P7) (or GFP, as a control) for rescue. *K, histograms* showing the quantification of relative protein levels for nectin-1 (*left*) or nectin-3 (*right*) in WT cells (*black column*), PLEKHA7-KO-1 clone (*dark gray*), KO-1 clone + GFP-PLEKHA7 rescue (*light gray*), KO-1 clone + GFP rescue (*very light gray*) shown as percentages of WT. *Histograms* were obtained from three separate experiments. *Asterisks* above columns indicate statistical significance.

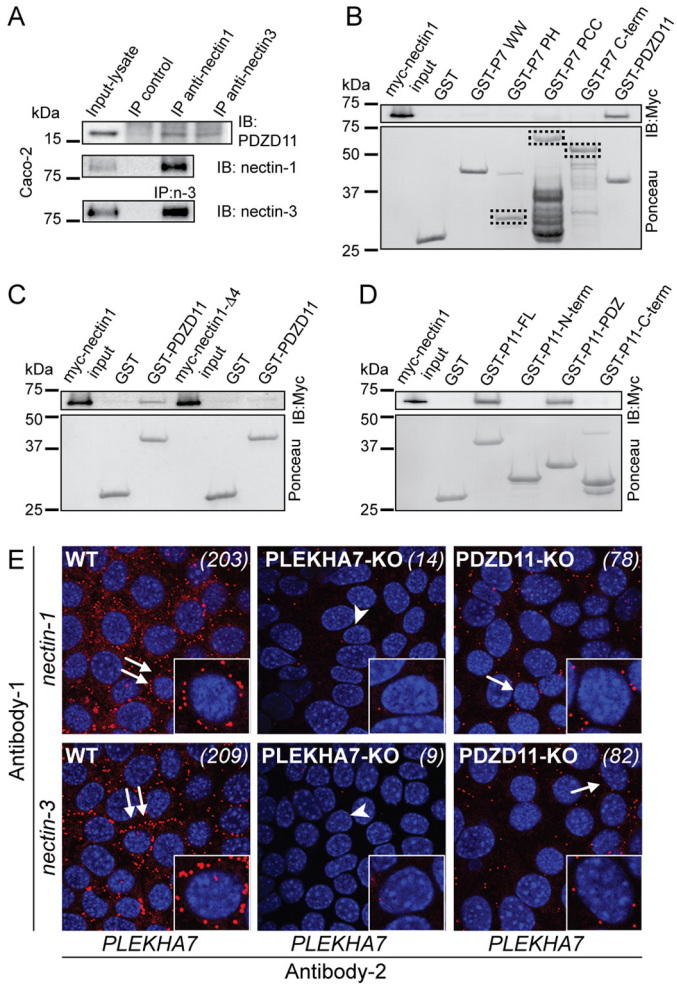


FIGURE 5. **Nectin forms a complex and interacts directly with PDZD11.** *A,* PDZD11 and nectins form a complex. Immunoblotting analysis of either nectin-1 or nectin-3 immunoprecipitates (from Caco2 whole cell lysates) with antibodies against PDZD11 (*top*), nectin-1 (*middle*), and nectin-3 (*bottom*). *B,* PDZD11 but not PLEKHA7 fragments interact directly with nectin-1. Immunoblotting analysis of GST pulldowns using either GST or GST fused to the following fragments of PLEKHA7: WW (residues 1–162, see Fig. 2); PH (residues 120–300); proline-rich and coiled-coil domains (PCC, residues 500–844); C-terminal (residues 821–1121 (7)), and Myc-tagged-nectin-1 as a prey. *Dotted boxes* indicate recombinant proteins stained by Ponceau-S. *C,* PDZD11 binds to the PDZ-binding motif of nectin-1. Immunoblotting analysis of GST pulldowns using either GST or GST-PDZD11 as baits and either Myc-tagged nectin-1 WT (Myc-nectin1) or the nectin-1 mutant lacking the last PDZ-binding motif 4 residues (Myc-nectin1-Δ4) (both expressed in HEK293T cells) as preys. The Ponceau-S-stained blot shows the amounts of recombinant proteins used as baits. *Numbers* on the *left* indicate size (kDa) and migration of prestained markers. *D,* PDZ domain of PDZD11 binds to nectin-1. Immunoblotting analysis of GST pulldowns using either GST or different fragments of PDZD11 (see Fig. 2) as baits, and Myc-tagged nectin-1 as a prey. *E,* detection of PDZD11-dependent PLEKHA7-nectin association by PLA. Cells were labeled with mouse anti-PLEKHA7 antibodies, and either rabbit anti-nectin-1 (*top panels*) or nectin-3 (*bottom panels*). Abundant brightly labeled dots along the regions of cell-cell contact are detected in WT cells (*double arrows* indicating WT cell shown in magnified *inset*); background labeling is detected in PLEKHA7-KO cells (*arrowhead* indicating PLEKHA7-KO cell shown in magnified *inset*), and decreased labeling (78 *versus* 203 dots for nectin-1 and 82 *versus* 209 dots for nectin-3) is detected in PDZD11-KO cells. Each panel is labeled with the cell genotype, and *numbers* in *italics* on the *top-right hand corner* of each image indicates number of fluorescent dots in the imaged field, for a semi-quantitative evaluation of assay results.

between PDZD11 and nectin, by biochemical direct *in vitro* binding assays. We show that the first WW domain of PLEKHA7 is sufficient for direct interaction with PDZD11 and that the 44-residue N-terminal sequence of PDZD11 interacts with PLEKHA7. Moreover, the PDZ-binding four-residue motif of nectin-1 mediates the interaction of nectin with the PDZ domain of PDZD11. The sequence of the P7-ID shows no homology to the N-terminal sequences of other single PDZ domain proteins and may function as a PDZ "supramodule," to allow higher specificity of interaction of PDZD11 with its target sequences (36). PLEKHA7 binding to this region may also modulate the affinity of binding of the PDZ domain of PDZD11 with its target sequences. Conversely, the P7-ID of PDZD11 comprises eight proline residues, including two PP (Pro-Pro) residues, but none of them shows a consensus ligand sequence belonging to any of the four previously identified WW-binding motif groups (37). Additional experiments are required to determine whether the proline motifs of PDZD11 define a new group of WW-interacting sequences and which residues of the WW1 domain of PLEKHA7 are implicated in its interaction with PDZD11. In summary, we assigned a specific protein-interaction function to the most N-terminal WW region of PLEKHA7, and we dissected the structure-function relationships in PDZD11.

PDZD11 was previously described as PISP, based on its binding to the cytoplasmic domain of all plasma membrane $Ca^{2+}$-ATPase b-splice variants (30). PDZD11 is also known as AIPP1 through its binding to the cytoplasmic tail of the Menkes copper ATPase ATP7A (31) and as an interactor of the sodium-dependent multivitamin transporter (32). The proposed function of PDZD11, a ubiquitously expressed protein, was to provide a scaffold for these transmembrane proteins, by binding through its PDZ domain, to the PDZ-binding motif at their C terminus. Supporting this idea, depletion of PDZD11 reduced the cell surface expression of the sodium-dependent multivitamin transporter, as assessed by cell surface biotinylation assay (32). Other single PDZ proteins, such as MALS (mammalian homolog of Lin-7), are implicated in intracellular transport and targeting of their partner proteins (38), and future studies should determine whether PDZD11 also plays this role, for example by promoting the efficient transport of PDZ-binding proteins such as nectins to the cell surface. Here, we discover a new role for PDZD11. It promotes the efficient recruitment and stabilization of nectins at AJ of epithelial cells. The C-terminal cytoplasmic domain of nectins interacts with the PDZ domains of several junctional partners as follows: afadin (35), which is important for the accumulation of nectin-1 at AJ (39), and depending on nectin isoform, also Par-3 (40), PICK-1 (41), MUPP1 (42), PATJ (42), and MPP3 (43). Therefore, redundant interactions can stabilize nectins at junctions (44). This is consistent with our observation that KO of PDZD11 in epithelial cells does not result in the complete loss of junctional nectins. PDZD11 may function not only through direct scaffolding of nectins but also indirectly by affecting the conformation of the N-terminal region of PLEKHA7, which interacts with afadin, hence affecting the PLEKHA7-afadin interaction and the ability of afadin to form an efficient scaffold for nectins.

Because PDZD11 promotes the efficient recruitment of nectins to ZA, we hypothesized that one cellular function of PDZD11 may be related to the function of nectins. Few studies have been carried out to address the function of nectins in cultured epithelial cells. Nectins independently initiate, subsequently followed by E-cadherin, the formation of AJ, by trans-

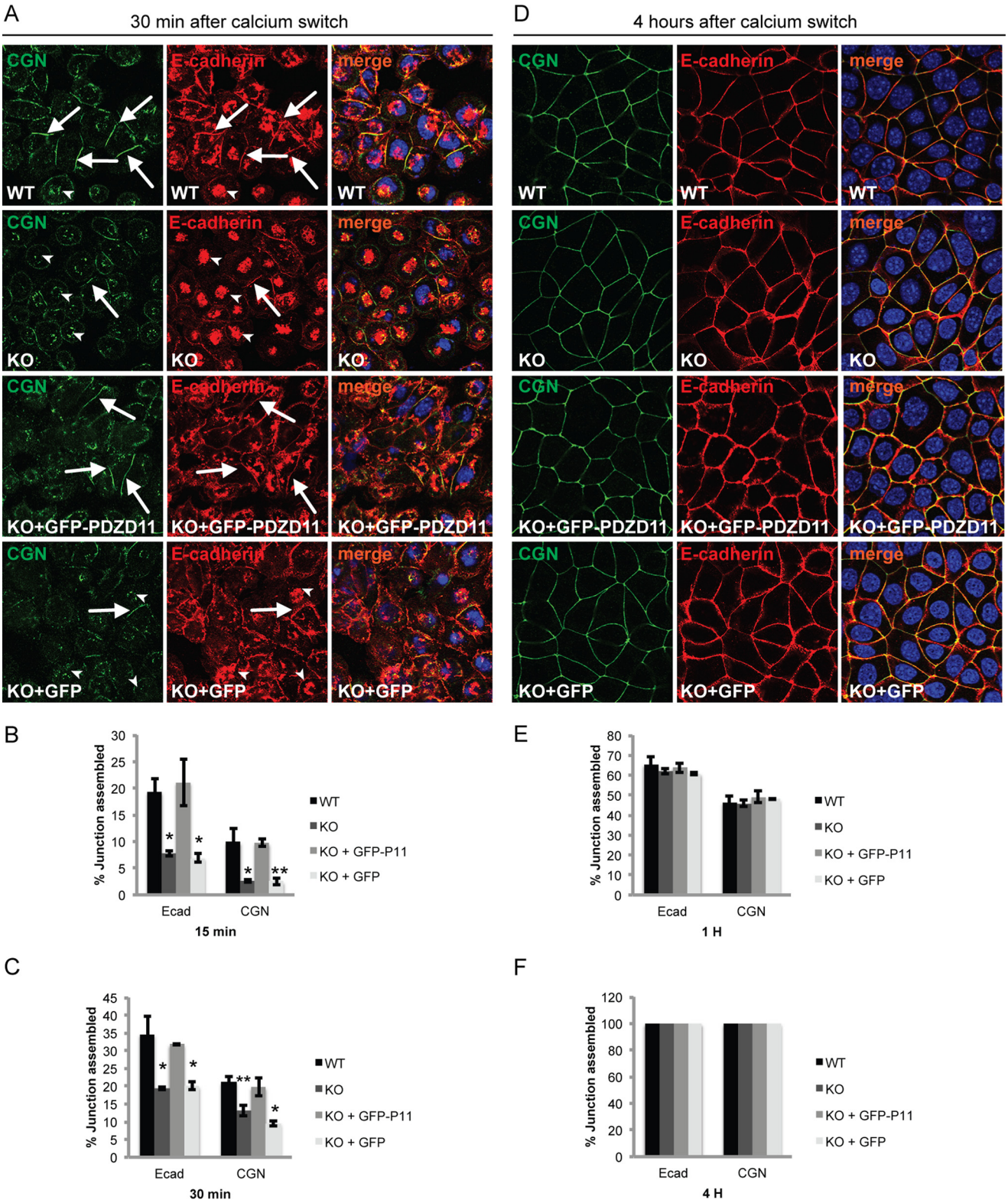


FIGURE 6. **PDZD11 is required for the efficient assembly of junctions at early time points after the calcium switch.** *A–C,* decreased junctional accumulation of E-cadherin and cingulin (*CGN*) at 15 and 30 min after the calcium switch. *A,* immunofluorescent localization of cingulin and E-cadherin in either WT cells (*1st row*), or PDZD11 KO cells (clone 2C7) (*2nd row*), or PDZD11 KO cells stably rescued with GFP-PDZD11 (*3rd row*), or PDZD11 KO cells stably rescued with GFP (*4th row*), 30 min after the calcium switch. *Arrows* indicate junctional labeling, and *arrowheads* indicate perinuclear granular labeling. *Merge* images show nuclei labeled in *blue* by DAPI. *B* and *C,* quantification of percent of junction assembly (see under "Experimental Procedures" for protocol) in WT cells (*black*), PDZD11 KO cells (*dark gray*), KO cells rescued with GFP-PDZD11 (*light gray*), KO cells rescued with GFP (*very light gray*), either 15 min (*B*) or 30 min (*C*) after the calcium switch. *D–F,* immunofluorescent localization of cingulin and E-cadherin 4 h after the calcium switch (*D*) and quantification of percent of junction assembly after either 1 h (*E*) or 4 h (*F*) after the calcium switch (see *A–C* for labeling). *Asterisks* indicate statistical significance (*, $p < 0.05$; **, $p < 0.01$).

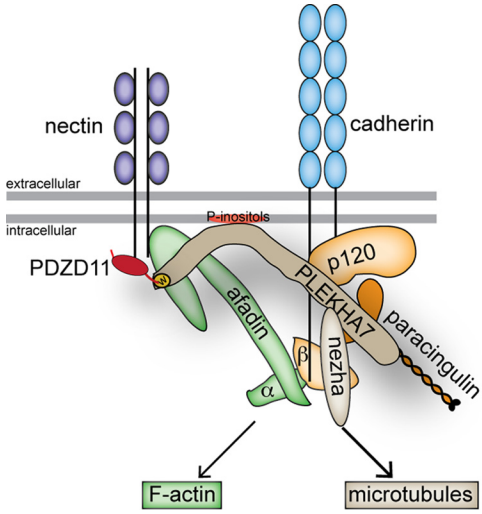


FIGURE 7. **New model of the molecular architecture of the *zonula adhaerens*.** This simplified scheme (depicting a half-junction) shows how PLEKHA7 may bridge nectin and cadherin complexes by binding through its N-terminal half to afadin and PDZD11, and through its C-terminal half to $p120^{Ctn}$ and paracingulin. The transmembrane ZA proteins nectin and E-cadherin are shown as dimers, with Ig-like and extracellular domains represented by *purple* and *blue ovals*, respectively. PLEKHA7 binds to its interactors $p120^{ctn}$ (6), paracingulin (CGNL1) (8), and nezha (6) through its central and C-terminal regions, to membrane-phosphorylated phosphatidylinositols (*orange patch*) through its PH domain (10), and to afadin (50) and PDZD11 through its N-terminal region. The *yellow circle* at the N terminus of PLEKHA7 indicates the WW1 domain (*w*) that is sufficient for PLEKHA7 interaction with PDZD11 *in vitro*. PDZD11 connects the C-terminal PDZ-binding motif of nectin to PLEKHA7. Afadin/α-catenin and nezha provide the linkage of the complexes to actin filaments and microtubules, respectively. The cytoplasmic domain of E-cadherin interacts with p120-catenin and β-catenin (which in turns binds to α-catenin).

interacting at protrusions of neighboring cells, giving rise to spot-like junctions that subsequently mature into belt-like AJ (45). Nectins and E-cadherin cooperatively organize AJ, by interacting through their cytoplasmic partners (46), although nectins can efficiently drive the formation of AJ and TJ even in the absence of E-cadherin (47). Nectin mutations that prevent their trans-interaction affect junction formation in MDCK cells, causing a delay in AJ formation (48). Consistent with the reduction of junctional nectin levels, and the role of nectins in initiating junction assembly, the KO of PDZD11 resulted in a reduction of the efficiency of assembly of zonular junctions, which was detectable at the 15- and 30-min time points in the calcium switch experimental model. Junction assembly resumed to normal kinetics at later time points in PDZD11-KO cells, probably due to the cooperative and redundant adhesive functions of E-cadherins and the residual nectin molecules.

We propose a new model for the architecture of the ZA (Fig. 7), based on the results presented here. By binding to p120-catenin and paracingulin on one side and to PDZD11 and afadin on the other side, PLEKHA7 establishes a molecular bridge between nectin- and cadherin-based protein complexes at the ZA (Fig. 7), distinct from the connection provided through the afadin-ponsin complex (49). Through PDZD11, PLEKHA7 contributes to recruiting nectins to the ZA. In addition, by binding both to afadin and to PDZD11, PLEKHA7 further strengthens the cytoplasmic scaffold for nectins, by bridging together these two cytoplasmic scaffolding proteins. Finally, by binding to actin filaments through afadin (and potentially other actin-binding proteins (17)), and to microtubules through nezha (6), PLEKHA7 contributes to reinforcing the cytoskeletal anchoring of both nectin and cadherin adhesion receptors.

The PLEKHA7-PDZD11 module that we describe provides a new type of molecular machinery that brings PDZ-binding membrane proteins to the AJ in epithelial and endothelial cells. This is important to explore new mechanistic hypotheses to understand at the molecular level the role of PLEKHA7 in tissue physiology and pathology. In fact, it has not escaped our attention that the interaction of PDZD11 with the plasma membrane $Ca^{2+}$-ATPase (30) may be relevant to the role of PLEKHA7 in the control of calcium homeostasis. Studies on zebrafish show that loss of the PLEKHA7 homologue *hadp1* leads to a reduced rate of extrusion of cytoplasmic $Ca^{2+}$ during diastole (10). Furthermore, in a model of PLEKHA7-KO rats, increased endothelial NOS signaling and increased intracellular calcium detected in PLEKHA7-KO aortic endothelial cells suggest that reduced blood pressure in KO animals may depend on PLEKHA7- and calcium-mediated increase of endothelial NOS signaling to vascular smooth muscle, leading to its relaxation (14). Significantly, both PDZD11 and PLEKHA7 are localized at endothelial junctions (Fig. 3*A*). Thus, we are currently investigating whether PLEKHA7 regulates plasma membrane $Ca^{2+}$-ATPase, and hence calcium homeostasis, through PDZD11, to clarify mechanistically its role in the regulation of blood pressure, cardiac contractility, and glaucoma. It is also possible that altered calcium homeostasis in PLEKHA7-KO cells underlies the phenotype of decreased susceptibility and recovery after intoxication by staphylococcal α-toxin, shown by cells and mice lacking PLEKHA7 (18). Interestingly, PDZD11 was one of the proteins identified in the screen on Hap1 cells whose KO reduced the cytotoxic effects of α-toxin (18).

In summary, here we describe a new protein complex module comprising PDZD11 and PLEKHA7, whereby the single PDZ domain protein PDZD11 connects nectins to the cadherin- and cytoskeleton-associated protein complex, through its binding to PLEKHA7 (Fig. 7), to stabilize nectins at AJ and promote efficient early assembly of junctions. The results presented here also raise the hypothesis that PLEKHA7 orchestrates the membrane organization and function of proteins regulating calcium homeostasis, through PDZD11, providing a new potential molecular mechanism to explain the implication of PLEKHA7 in vascular and cardiac pathophysiology.

*Author Contributions*—D. G. characterized anti-PDZD11 antibodies, carried out immunofluorescence, immunoprecipitation, and pulldown analyses, and generated and characterized PDZD11-KO mCCD cells. J. S. generated PLEKHA7-KO mCCD cells and rescue cells and constructs, characterized anti-PLEKHA7 antibodies, and carried out immunofluorescence and pulldown analyses. E. V. and S. S. carried out immunoblotting, immunofluorescence, and immunoprecipitation analysis of additional cultured cell lines. I. M. and L. J. generated cDNA constructs and helped in recombinant protein expression, GST pulldown, and immunoblotting experiments. I. P., M. M., and A. A. H. conducted QUBIC experiments. S. C. initiated, organized, and supervised the project. D. G., J. S., and S. C. analyzed the data. S. C. wrote the paper.

*Acknowledgments—We thank all the colleagues cited in the text for their kind gift of cell lines and reagents.*

**References**


1. Anderson, J. M., and Van Itallie, C. M. (2009) Physiology and function of the tight junction. *Cold Spring Harb. Perspect. Biol.* **1,** a002584
2. Takeichi, M. (2014) Dynamic contacts: rearranging adherens junctions to drive epithelial remodelling. *Nat. Rev. Mol. Cell Biol.* **15,** 397–410
3. Harris, T. J., and Tepass, U. (2010) Adherens junctions: from molecules to morphogenesis. *Nat. Rev. Mol. Cell Biol.* **11,** 502–514
4. McCrea, P. D., Gu, D., and Balda, M. S. (2009) Junctional music that the nucleus hears: cell-cell contact signaling and the modulation of gene activity. *Cold Spring Harb. Perspect. Biol.* **1,** a002923
5. Mandai, K., Rikitake, Y., Mori, M., and Takai, Y. (2015) Nectins and nectin-like molecules in development and disease. *Curr. Top. Dev. Biol.* **112,** 197–231
6. Meng, W., Mushika, Y., Ichii, T., and Takeichi, M. (2008) Anchorage of microtubule minus ends to adherens junctions regulates epithelial cell-cell contacts. *Cell* **135,** 948–959
7. Pulimeno, P., Bauer, C., Stutz, J., and Citi, S. (2010) PLEKHA7 is an adherens junction protein with a tissue distribution and subcellular localization distinct from ZO-1 and E-cadherin. *PLoS ONE* **5,** e12207
8. Pulimeno, P., Paschoud, S., and Citi, S. (2011) A role for ZO-1 and PLEKHA7 in recruiting paracingulin to tight and adherens junctions of epithelial cells. *J. Biol. Chem.* **286,** 16743–16750
9. Citi, S., Pulimeno, P., and Paschoud, S. (2012) Cingulin, paracingulin, and PLEKHA7: signaling and cytoskeletal adaptors at the apical junctional complex. *Ann. N.Y. Acad. Sci.* **1257,** 125–132
10. Wythe, J. D., Jurynec, M. J., Urness, L. D., Jones, C. A., Sabeh, M. K., Werdich, A. A., Sato, M., Yost, H. J., Grunwald, D. J., Macrae, C. A., and Li, D. Y. (2011) Hadp1, a newly identified pleckstrin homology domain protein, is required for cardiac contractility in zebrafish. *Dis. Model. Mech.* **4,** 607–621
11. Levy, D., Ehret, G. B., Rice, K., Verwoert, G. C., Launer, L. J., Dehghan, A., Glazer, N. L., Morrison, A. C., Johnson, A. D., Aspelund, T., Aulchenko, Y., Lumley, T., Köttgen, A., Vasan, R. S., Rivadeneira, F., *et al.* (2009) Genome-wide association study of blood pressure and hypertension. *Nat. Genet.* **41,** 677–687
12. Hong, K. W., Jin, H. S., Lim, J. E., Kim, S., Go, M. J., and Oh, B. (2010) Recapitulation of two genome-wide association studies on blood pressure and essential hypertension in the Korean population. *J. Hum. Genet.* **55,** 336–341
13. Lin, Y., Lai, X., Chen, B., Xu, Y., Huang, B., Chen, Z., Zhu, S., Yao, J., Jiang, Q., Huang, H., Wen, J., and Chen, G. (2011) Genetic variations in CYP17A1, CACNB2 and PLEKHA7 are associated with blood pressure and/or hypertension in the ethnic minority of China. *Atherosclerosis* **219,** 709–714
14. Endres, B. T., Priestley, J. R., Palygin, O., Flister, M. J., Hoffman, M. J., Weinberg, B. D., Grzybowski, M., Lombard, J. H., Staruschenko, A., Moreno, C., Jacob, H. J., and Geurts, A. M. (2014) Mutation of Plekha7 attenuates salt-sensitive hypertension in the rat. *Proc. Natl. Acad. Sci. U.S.A.* **111,** 12817–12822
15. Vithana, E. N., Khor, C. C., Qiao, C., Nongpiur, M. E., George, R., Chen, L. J., Do, T., Abu-Amero, K., Huang, C. K., Low, S., Tajudin, L. S., Perera, S. A., Cheng, C. Y., Xu, L., Jia, H., *et al.* (2012) Genome-wide association analyses identify three new susceptibility loci for primary angle closure glaucoma. *Nat. Genet.* **44,** 1142–1146
16. Chen, Y., Chen, X., Wang, L., Hughes, G., Qian, S., and Sun, X. (2014) Extended association study of PLEKHA7 and COL11A1 with primary angle closure glaucoma in a Han Chinese population. *Invest. Ophthalmol. Vis. Sci.* **55,** 3797–3802
17. Kourtidis, A., Ngok, S. P., Pulimeno, P., Feathers, R. W., Carpio, L. R., Baker, T. R., Carr, J. M., Yan, I. K., Borges, S., Perez, E. A., Storz, P., Copland, J. A., Patel, T., Thompson, E. A., Citi, S., and Anastasiadis, P. Z. (2015) Distinct E-cadherin-based complexes regulate cell behaviour through miRNA processing or Src and p120 catenin activity. *Nat. Cell Biol.* **17,** 1145–1157
18. Popov, L. M., Marceau, C. D., Starkl, P. M., Lumb, J. H., Shah, J., Guerrera, D., Cooper, R. L., Merakou, C., Bouley, D. M., Meng, W., Kiyonari, H., Takeichi, M., Galli, S. J., Bagnoli, F., Citi, S., *et al.* (2015) The adherens junctions control susceptibility to *Staphylococcus aureus* α-toxin. *Proc. Natl. Acad. Sci. U.S.A.* **112,** 14337–14342
19. Cardellini, P., Davanzo, G., and Citi, S. (1996) Tight junctions in early amphibian development: detection of junctional cingulin from the 2-cell stage and its localization at the boundary of distinct membrane domains in dividing blastomeres in low calcium. *Dev. Dyn.* **207,** 104–113
20. Paschoud, S., Yu, D., Pulimeno, P., Jond, L., Turner, J. R., and Citi, S. (2011) Cingulin and paracingulin show similar dynamic behaviour, but are recruited independently to junctions. *Mol. Membr. Biol.* **28,** 123–135
21. Paschoud, S., Jond, L., Guerrera, D., and Citi, S. (2014) PLEKHA7 modulates epithelial tight junction barrier function. *Tissue Barriers* **2,** e28755
22. Poser, I., Sarov, M., Hutchins, J. R., Hériché, J. K., Toyoda, Y., Pozniakovsky, A., Weigl, D., Nitzsche, A., Hegemann, B., Bird, A. W., Pelletier, L., Kittler, R., Hua, S., Naumann, R., Augsburg, M., *et al.* (2008) BAC TransgeneOmics: a high-throughput method for exploration of protein function in mammals. *Nat. Methods* **5,** 409–415
23. Hubner, N. C., and Mann, M. (2011) Extracting gene function from protein-protein interactions using Quantitative BAC InteraCtomics (QUBIC). *Methods* **53,** 453–459
24. Cordenonsi, M., D'Atri, F., Hammar, E., Parry, D. A., Kendrick-Jones, J., Shore, D., and Citi, S. (1999) Cingulin contains globular and coiled-coil domains and interacts with ZO-1, ZO-2, ZO-3, and myosin. *J. Cell Biol.* **147,** 1569–1582
25. Citi, S., D'Atri, F., Cordenonsi, M., and Cardellini, P. (2001) in *Cell-Cell Interactions* (Fleming, T. P., ed) pp. 153–176, 2nd Ed., IRL Press, Oxford
26. Paschoud, S., and Citi, S. (2008) Inducible overexpression of cingulin in stably transfected MDCK cells does not affect tight junction organization and gene expression. *Mol. Membr. Biol.* **25,** 1–13
27. Guillemot, L., Guerrera, D., Spadaro, D., Tapia, R., Jond, L., and Citi, S. (2014) MgcRacGAP interacts with cingulin and paracingulin to regulate Rac1 activation and development of the tight junction barrier during epithelial junction assembly. *Mol. Biol. Cell* **25,** 1995–2005
28. Spadaro, D., Tapia, R., Jond, L., Sudol, M., Fanning, A. S., and Citi, S. (2014) ZO proteins redundantly regulate the transcription factor DbpA/ZONAB. *J. Biol. Chem.* **289,** 22500–22511
29. Martinez-Palomo, A., Meza, I., Beaty, G., and Cereijido, M. (1980) Experimental modulation of occluding junctions in a cultured transporting epithelium. *J. Cell Biol.* **87,** 736–745
30. Goellner, G. M., DeMarco, S. J., and Strehler, E. E. (2003) Characterization of PISP, a novel single-PDZ protein that binds to all plasma membrane $Ca^{2+}$-ATPase b-splice variants. *Ann. N.Y. Acad. Sci.* **986,** 461–471
31. Stephenson, S. E., Dubach, D., Lim, C. M., Mercer, J. F., and La Fontaine, S. (2005) A single PDZ domain protein interacts with the Menkes copper ATPase, ATP7A. A new protein implicated in copper homeostasis. *J. Biol. Chem.* **280,** 33270–33279
32. Nabokina, S. M., Subramanian, V. S., and Said, H. M. (2011) Association of PDZ-containing protein PDZD11 with the human sodium-dependent multivitamin transporter. *Am. J. Physiol. Gastrointest. Liver Physiol.* **300,** G561–G567
33. Shah, J., Guerrera, D., Vasileva, E., Sluysmans, S., Bertels, E., and Citi, S. (2016) PLEKHA7: cytoskeletal adaptor protein at center stage in junctional organization and signaling. *Int. J. Biochem. Cell Biol.* **75,** 112–116
34. Miyahara, M., Nakanishi, H., Takahashi, K., Satoh-Horikawa, K., Tachibana, K., and Takai, Y. (2000) Interaction of nectin with afadin is necessary for its clustering at cell-cell contact sites but not for its cis dimerization or trans interaction. *J. Biol. Chem.* **275,** 613–618
35. Takahashi, K., Nakanishi, H., Miyahara, M., Mandai, K., Satoh, K., Satoh, A., Nishioka, H., Aoki, J., Nomoto, A., Mizoguchi, A., and Takai, Y. (1999) Nectin/PRR: an immunoglobulin-like cell adhesion molecule recruited to cadherin-based adherens junctions through interaction with Afadin, a PDZ domain-containing protein. *J. Cell Biol.* **145,** 539–549
36. Ye, F., and Zhang, M. (2013) Structures and target recognition modes of PDZ domains: recurring themes and emerging pictures. *Biochem. J.* **455,** 1–14
37. Sudol, M., Sliwa, K., and Russo, T. (2001) Functions of WW domains in the nucleus. *FEBS Lett.* **490,** 190–195
38. Zhang, J., Yang, X., Wang, Z., Zhou, H., Xie, X., Shen, Y., and Long, J. (2012) Structure of an L27 domain heterotrimer from cell polarity com-

plex Patj/Pals1/Mals2 reveals mutually independent L27 domain assembly mode. *J. Biol. Chem.* **287,** 11132–11140
39. Ishiuchi, T., and Takeichi, M. (2012) Nectins localize Willin to cell-cell junctions. *Genes Cells* **17,** 387–397
40. Takekuni, K., Ikeda, W., Fujito, T., Morimoto, K., Takeuchi, M., Monden, M., and Takai, Y. (2003) Direct binding of cell polarity protein PAR-3 to cell-cell adhesion molecule nectin at neuroepithelial cells of developing mouse. *J. Biol. Chem.* **278,** 5497–5500
41. Reymond, N., Garrido-Urbani, S., Borg, J. P., Dubreuil, P., and Lopez, M. (2005) PICK-1: a scaffold protein that interacts with Nectins and JAMs at cell junctions. *FEBS Lett.* **579,** 2243–2249
42. Adachi, M., Hamazaki, Y., Kobayashi, Y., Itoh, M., Tsukita, S., Furuse, M., and Tsukita, S. (2009) Similar and distinct properties of MUPP1 and Patj, two homologous PDZ domain-containing tight-junction proteins. *Mol. Cell. Biol.* **29,** 2372–2389
43. Dudak, A., Kim, J., Cheong, B., Federoff, H. J., and Lim, S. T. (2011) Membrane palmitoylated proteins regulate trafficking and processing of nectins. *Eur. J. Cell Biol.* **90,** 365–375
44. Rikitake, Y., Mandai, K., and Takai, Y. (2012) The role of nectins in different types of cell-cell adhesion. *J. Cell Sci.* **125,** 3713–3722
45. Asakura, T., Nakanishi, H., Sakisaka, T., Takahashi, K., Mandai, K., Nishimura, M., Sasaki, T., and Takai, Y. (1999) Similar and differential behaviour between the nectin-afadin-ponsin and cadherin-catenin systems during the formation and disruption of the polarized junctional alignment in epithelial cells. *Genes Cells* **4,** 573–581
46. Tachibana, K., Nakanishi, H., Mandai, K., Ozaki, K., Ikeda, W., Yamamoto, Y., Nagafuchi, A., Tsukita, S., and Takai, Y. (2000) Two cell adhesion molecules, nectin and cadherin, interact through their cytoplasmic domain-associated proteins. *J. Cell Biol.* **150,** 1161–1176
47. Fukuhara, A., Irie, K., Yamada, A., Katata, T., Honda, T., Shimizu, K., Nakanishi, H., and Takai, Y. (2002) Role of nectin in organization of tight junctions in epithelial cells. *Genes Cells* **7,** 1059–1072
48. Hoshino, T., Shimizu, K., Honda, T., Kawakatsu, T., Fukuyama, T., Nakamura, T., Matsuda, M., and Takai, Y. (2004) A novel role of nectins in inhibition of the E-cadherin-induced activation of Rac and formation of cell-cell adherens junctions. *Mol. Biol. Cell* **15,** 1077–1088
49. Mandai, K., Nakanishi, H., Satoh, A., Takahashi, K., Satoh, K., Nishioka, H., Mizoguchi, A., and Takai, Y. (1999) Ponsin/SH3P12: an l-afadin- and vinculin-binding protein localized at cell-cell and cell-matrix adherens junctions. *J. Cell Biol.* **144,** 1001–1017
50. Kurita, S., Yamada, T., Rikitsu, E., Ikeda, W., and Takai, Y. (2013) Binding between the junctional proteins afadin and PLEKHA7 and implication in the formation of adherens junction in epithelial cells. *J. Biol. Chem.* **288,** 29356–29368